# Time-dependent and time-independent close-coupling methods for the electron-impact ionization of $Be^+$

M. S. Pindzola and F. Robicheaux
*Department of Physics, Auburn University, Auburn, Alabama 36849*

N. R. Badnell
*Department of Physics and Applied Physics, University of Strathclyde, Glasgow G4 0NG, United Kingdom*

T. W. Gorczyca
*Department of Physics, Western Michigan University, Kalamazoo, Michigan 49008*
(Received 3 March 1997)

The electron-impact ionization cross section of $Be^+$ is calculated using both a time-dependent and a time-independent close-coupling method. The time-dependent method is based on the propagation of wave packets constructed using excited-state orbitals calculated in a core pseudopotential. The time-independent method is an $R$-matrix solution based on a total wave function constructed using antisymmetrized products of Laguerre pseudo-orbitals and zero-derivative box orbitals. In both methods, low partial-wave close-coupling results are added to high partial-wave distorted-wave results to yield ionization cross sections for $Be^+$ substantially below the experimental crossed-beam measurements of Falk and Dunn [Phys. Rev. A **27**, 754 (1983)] and in agreement with the recent time-independent close-coupling calculations of Bartschat and Bray [J. Phys. B **30**, L109 (1997)]. [S1050-2947(97)07809-8]

PACS number(s): 34.80.Kw

## I. INTRODUCTION

Recently, several *ab initio* theoretical methods have been developed that have the capability of producing accurate electron-impact ionization cross sections for atoms and their ions. The converged close-coupling [1], the hyperspherical close-coupling [2], the $R$-matrix with pseudostates [3], and the time-dependent close-coupling [4,5] methods have all produced ionization cross sections for hydrogen in excellent agreement with experiment [6]. The converged close-coupling [7] and $R$-matrix with pseudostates [8] methods have also produced accurate cross sections for the electron-impact ionization of helium. Since accurate electron-impact ionization cross sections for atomic ions are needed for the modeling of a variety of laboratory and astrophysical plasmas, it is important to extend the range of atomic systems that can be treated by these advanced methods.

When Bray [9] extended the converged close-coupling method to calculate electron ionization cross sections for low-charge ions in the Li isoelectronic sequence, he found serious discrepancies between theory and crossed-beam experiments on $Be^+$ [10], $B^{2+}$ [11], and $C^{3+}$ [12]. Very recently Bartschat and Bray [13] repeated the converged close-coupling calculations and carried out $R$-matrix with pseudostates calculations for the ionization of $Be^+$ and again found a serious discrepancy between theory and experiment. In this paper we apply the quite different time-dependent close-coupling method to calculate the electron-impact ionization of $Be^+$, while at the same time carrying out an $R$-matrix calculation using a large pseudostate basis and a continuum basis set orthogonalization procedure. The time-dependent close-coupling method is based on the propagation of wave packets and their projection onto a complete set of bound excited states. To go beyond our previous work on electron ionization of hydrogen, we calculate the excited-state spectrum using a pseudopotential for the core electrons. The pseudopotential method has the added benefits of keeping the lattice size relatively small and eliminating problems with superelastic scattering. The time-independent close-coupling method is based on an $R$-matrix solution with Laguerre pseudostates. In contrast to the use of Gram-Schmidt methods, orthogonality between the different sets of orbitals needed to construct the scattering wave function is obtained by diagonalizing the matrix of overlaps. In both methods, low partial-wave close-coupling results are added to high partial-wave distorted-wave results to obtain the total ionization cross section for $Be^+$. As will be shown, our sets of results confirm the time-independent close-coupling calculations of Bray [9] and Bartschat and Bray [13] and are thus substantially below the experimental crossed-beams measurements of Falk and Dunn [10]. The time-dependent theory is reviewed in Sec. II, the time-independent theory is reviewed in Sec. III, the two methods are compared with each other and experiment in Sec. IV, and a brief summary is found in Sec. V.

## II. TIME-DEPENDENT THEORY

For electron scattering from atomic ions involving one electron outside a closed shell, the time-dependent close-coupling equations for each $LS$ symmetry are given by (in atomic units)

 

$$i\frac{\partial P^{LS}_{l_1 l_2}(r_1,r_2,t)}{\partial t}=T_{l_1 l_2}(r_1,r_2)P^{LS}_{l_1 l_2}(r_1,r_2,t)+\sum_{l_1',l_2'}V^{L}_{l_1 l_2,l_1' l_2'}(r_1,r_2)P^{LS}_{l_1' l_2'}(r_1,r_2,t), \tag{1}$$

where

$$T_{l_1 l_2}(r_1,r_2)=-\frac{1}{2}\frac{\partial^2}{\partial r_1^2}-\frac{1}{2}\frac{\partial^2}{\partial r_2^2}+V^{l_1}_{PP}(r_1)+V^{l_2}_{PP}(r_2), \tag{2}$$

$V^{l}_{PP}$ is an $l$-dependent core pseudopotential, and the coupling operator $V^{L}_{l_1 l_2,l_1' l_2'}$ is given by

$$V^{L}_{l_1 l_2,l_1' l_2'}(r_1,r_2)=(-1)^{L+l_2+l_2'}\sqrt{(2l_1+1)(2l_1'+1)(2l_2+1)(2l_2'+1)}\sum_{\lambda}\frac{r_<^{\lambda}}{r_>^{\lambda+1}}\begin{pmatrix} l_1 & \lambda & l_1' \\ 0 & 0 & 0\end{pmatrix}\begin{pmatrix} l_2 & \lambda & l_2' \\ 0 & 0 & 0\end{pmatrix}\begin{Bmatrix} L & l_2' & l_1' \\ \lambda & l_1 & l_2\end{Bmatrix}. \tag{3}$$

The coupled partial differential equations are solved on a two-dimensional lattice using an explicit time propagator. At time $t=0$ the wave function $P^{LS}_{l_1 l_2}(r_1,r_2,0)$ is constructed as a symmetric product of an incoming radial wave packet for the scattering electron and a bound radial orbital $P_{nl}(r)$ for the valence electron. Following the collision at time $t=T$, the spin-averaged electron-impact ionization cross section is given by

$$\sigma_{\rm ion}=\frac{\pi}{4k^2}\sum_{L,S}(2L+1)(2S+1)\wp^{LS}_{\rm ion}, \tag{4}$$

where

$$\wp^{LS}_{\rm ion}=1-\sum_{n,l}\delta(l_1 l L)\int_0^{\infty}dr_1\left[\int_0^{\infty}dr_2 P^{LS}_{l_1 l}(r_1,r_2,T)P_{nl}(r_2)\right]^2-\sum_{n,l}\delta(l l_2 L)\int_0^{\infty}dr_2\left[\int_0^{\infty}dr_1 P^{LS}_{l l_2}(r_1,r_2,T)P_{nl}(r_1)\right]^2$$
$$+\sum_{n,l}\sum_{n',l'}\delta(l l' L)\left[\int_0^{\infty}dr_1\int_0^{\infty}dr_2 P^{LS}_{l l'}(r_1,r_2,T)P_{nl}(r_1)P_{n' l'}(r_2)\right]^2 \tag{5}$$

and $\delta(l_1 l_2 l_3)$ is an algebraic triangle relation.

The closed-shell orbitals are obtained by solving their corresponding Hartree-Fock equations [14]. The core orbitals are then used to construct the radial Hamiltonian

$$h(r)=-\frac{1}{2}\frac{\partial^2}{\partial r^2}+V^{l}_{HX}(r), \tag{6}$$

where

$$V^{l}_{HX}(r)=\frac{l(l+1)}{2r^2}-\frac{Z}{r}+V_H(r)-\frac{\alpha_l}{2}\left(\frac{24\rho}{\pi}\right)^{1/3}, \tag{7}$$

$V_H(r)$ is the Hartree potential, and $\rho$ is the probability density. The excited-state spectrum is obtained by diagonalizing $h(r)$ on the lattice. The parameter $\alpha_l$ is varied to obtain experimental energy splittings for the first few excited states.

If we choose the model potential $V^{l}_{HX}$ instead of $V_{PP}$ in Eq. (2), we run into problems associated with superelastic scattering. This is best illustrated with a sample $^1S$ partial-wave calculation for the electron-impact ionization of $Be^+$ at an incident energy of 50 eV. The absolute value squared of $P^{00}_{ss}(r_1,r_2,t=0)$ for the $2s$ ground state of $Be^+$ is shown in Fig. 1(a). The radial wave packet for the scattering electron is centered at $r=20.0$, while the second antinode for the $P_{2s}(r)$ orbital peaks at about $r=2.0$. The inner node of the $2s$ orbital is clearly seen in the contour plot. Following the time propagation of the three-channel close-coupled equations, the absolute value squared of $P^{00}_{ss}(r_1,r_2,t=20)$ is shown in Fig. 1(b). Of interest to us here is the probability density for $r<1.0$ along each axis. The probability flow in this region is fast, having already been reflected from the lattice boundary. It represents excitation from $2s\rightarrow 1s$. Since the $1s$ orbital is already filled, the use of a model potential in the time-dependent equations has generated an unphysical result.

To solve this problem we introduce pseudopotentials into the time-dependent method. Using standard procedures [15], we first generate a lowest-energy pseudo-orbital for each angular momentum occupied in the core. Essentially all the inner nodes of the previously generated lowest-energy valence orbital are removed in a smooth manner. An $l$-dependent pseudopotential is obtained by inverting the radial Schrödinger equation with the newly constructed pseudo-orbital. The new radial Hamiltonian

$$h(r)=-\frac{1}{2}\frac{\partial^2}{\partial r^2}+V^{l}_{PP}(r) \tag{8}$$

is then diagonalized on the lattice to obtain an excited pseu-

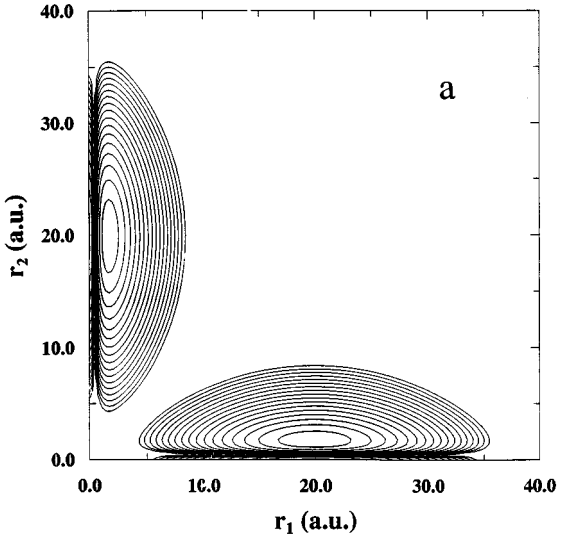


FIG. 1. $^1S$ partial-wave probability densities for electron-impact ionization of $Be^+$ at 50.0 eV using a model potential: (a) contour plot for $|P_{ss}^{00}(r_1,r_2,t=0)|^2$ and (b) contour plot for $|P_{ss}^{00}(r_1,r_2,t=20)|^2$.

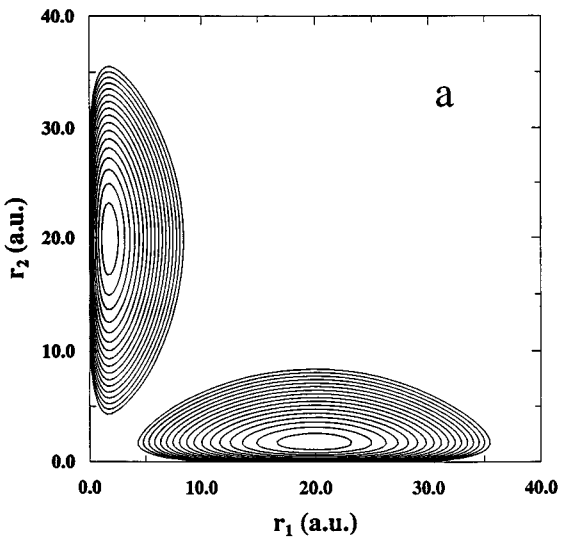


FIG. 2. $^1S$ partial-wave probability densities for electron-impact ionization of $Be^+$ at 50.0 eV using a model pseudopotential: (a) contour plot for $|P_{ss}^{00}(r_1,r_2,t=0)|^2$ and (b) contour plot for $|P_{ss}^{00}(r_1,r_2,t=20)|^2$.

dostate spectrum. For $Be^+$ the $ns$ radial orbital spectrum is replaced with an $\overline{ns}$ radial pseudo-orbital spectrum. The absolute value squared of $P_{ss}^{00}(r_1,r_2,t=0)$ for the $2\overline{s}$ ground state of $Be^+$ is shown in Fig. 2(a). The $2\overline{s}$ pseudo-orbital does not have an inner node, as is clearly seen in the contour plot. Following the time propagation of the three-channel close-coupled equations, the absolute value squared of $P_{ss}^{00}(r_1,r_2,t=20)$ is shown in Fig. 2(b). The unphysical superelastic scattering problem has been eliminated.

The time-dependent close-coupling equations were solved for electron scattering from $Be^+$ at incident energies of 40, 50, and 60 eV. We employed a $200\times200$ lattice with each radial direction from 0 to 40 spanned by a uniform mesh with spacing $\Delta r=0.20$. Between 3600 and 9200 time steps were needed to propagate each of the 12 $LS$ symmetric wave packets before cross-section convergence was achieved. The number of coupled partial differential equations ranged from 4 for the $^1S$ wave packet to 16 for the $^3H$ wave packet.

## III. TIME-INDEPENDENT THEORY

We use an $L^2$ basis to represent the bound and continuum states of the ion [16]. Excitation of the positive energy states corresponds to ionization [17]. We use the program AUTOSTRUCTURE [18] to generate an orthogonal set of Laguerre basis orbitals by Schmidt orthogonalizing the nonorthogonal basis

$$P_{nl}(r)=N_{nl}(\lambda_{nl}Zr)^{l+1}e^{-\lambda_{nl}Zr/2}L_{n+l}^{2l+1}(\lambda_{nl}Zr). \qquad (9)$$

Here $L_{n+l}^{2l+1}$ denotes an associated Laguerre polynomial and $N_{nl}$ is a normalization constant. We note that the scaling parameter $\lambda_{nl}$ does not include the charge $Z$; here $Z=z+1$, where $z$ is the residual charge on the ion. We take all of the $\lambda_{nl}$ to be equal to unity in all of our calculations since we find that this value minimizes the size of the pseudoresonance structure, i.e., it speeds up the convergence of the pseudostate expansion. We use physical orbitals for those states that we wish to study transitions between, or from,

rather than rely on using a large enough set of Laguerre states so as to converge to the physical ones. The $N$-electron configurations are built up from the one-electron orbitals and then the Hamiltonian is diagonalized to obtain the set of $N$-electron eigenenergies and eigenstates. For $Be^+$, we use physical $1s$, $2s$, and $2p$ orbitals and pseudo-orbitals for $n=3-12$, $l=0-3$ since we concern ourselves purely with ionization. This gives us six pseudostates per angular momentum that lie in the continuum. We investigated also the effect of adding eight $g$ states and found it to be negligible ($\sim 1\%$) for the total ionization cross section. Thus our $R$-matrix pseudostate basis is much larger than that of Bartschat and Bray [13]. They were looking at excitation (up to $n=4$) as well as ionization and so used physical (Hartree-Fock) orbitals up to $n=4$ and pseudo-orbitals that gave only three $s$ states, three $p$ states, two $d$ states, and one $f$ state lying in the continuum. This limited pseudostate expansion necessitated taking the average of results obtained from six separate $R$-matrix runs using different scaling parameters. It also necessitated a further correction to the ionization cross section to allow for the contribution to ionization from excitation to bound pseudostates. In fact, our $R$-matrix calculations are much closer in spirit to the convergent close-coupling calculations of Bray [9] and Bartschat and Bray [13]. Indeed, our pseudostate expansion including the $g$ states is the same size as that used by Bray [9]. Finally, a larger convergent close-coupling expansion was used by Bartschat and Bray [13] (to $n=15$) so as to obtain convergence of the ($n=4$) pseudostates to the physical $n=4$ states.

We solve the time-independent close-coupling equations using the $R$-matrix method [19]. Our starting point is RMATRIX I, the Breit-Pauli $R$-matrix codes [20] developed for the Iron Project [21]. The Laguerre basis orbitals are ideal since the functions and their first derivatives vanish at the $R$-matrix boundary, just like the physical orbitals. A practical problem encountered is the orthogonalization of the continuum basis orbitals, which are used to describe the scattering electron, to the Laguerre orbitals. Bartschat *et al.* [22] used a numerical Schmidt orthogonalization procedure. We use an alternative approach that we find to be more stable numerically when using a large $R$-matrix continuum basis [23,24]. Initially we have two distinct sets of orthonormal orbitals, namely, the physical plus pseudo-orbitals, which we denote by $\overline{\mathbf{p}}$, and the continuum basis orbitals, which we denote by $\underline{\mathbf{u}}$. We now form a single orthonormal set $\mathbf{v}$, which consists of $\overline{\mathbf{p}}$ plus a new continuum basis $\underline{\mathbf{u}}$, as follows: write $\underline{\mathbf{u}}=\mathbf{a}\overline{\mathbf{p}}+\mathbf{b}\underline{\mathbf{u}}$; then $\mathbf{v}$ is orthonormal if $\mathbf{a}=-\mathbf{b}\mathbf{M}$ and $\mathbf{b}=\mathbf{d}^{-1/2}\mathbf{O}^T$. Here $\mathbf{M}$ is the matrix of overlap integrals between $\underline{\mathbf{u}}$ and $\overline{\mathbf{p}}$ [$\{\mathbf{M}\}_{ij}=\int dr\, u_i(r)\overline{p_j}(r)$], $\mathbf{O}$ is the matrix that diagonalizes $\mathbf{I}-\mathbf{M}\mathbf{M}^T$ ($\mathbf{O}^T[\mathbf{I}-\mathbf{M}\mathbf{M}^T]\mathbf{O}=\mathbf{d}$), and $\mathbf{d}$ is the associated diagonal eigenvalue matrix. Eigenvalues of zero correspond to linear combinations of the $\mathbf{u}$ basis that are spanned by the $\overline{\mathbf{p}}$ basis and these are neglected (in practice, we keep those with eigenvalues greater than $10^{-4}$, which we find is more than sufficient to avoid any numerical instability). Thus, in general, the new continuum basis $\underline{\mathbf{u}}$ contains fewer orbitals than the original $\mathbf{u}$ basis. However, care must be taken in evaluating the Buttle correction since the effective one-body Hamiltonian is not diagonal in $\mathbf{v}$, and so we diagonalize it. We then recover the original eigenenergies and surface amplitudes of the $\mathbf{u}$ basis plus some extra ones corresponding to that part of the $\mathbf{v}$ basis that is spanned by $\overline{\mathbf{p}}$, not by $\mathbf{u}$. This procedure for obtaining a continuum basis that is orthogonal to the physical plus pseudo-orbital basis is completely automatic and numerically stable with large numbers of pseudo-orbitals and continuum basis orbitals: up to 15 of the former and 80 of the latter per angular momentum have been tested. For $Be^+$, our ''target'' orbitals necessitate the use of an $R$-matrix box of radius $R=37$ and this means that with 40 continuum basis orbitals per angular momentum (initially) we can go up to an incident electron energy of 80 eV. We carried out $LS$-coupling calculations, as described above, for $L=0-8$ with a small ''top up'' for higher $L$ obtained from the distorted-wave calculations.

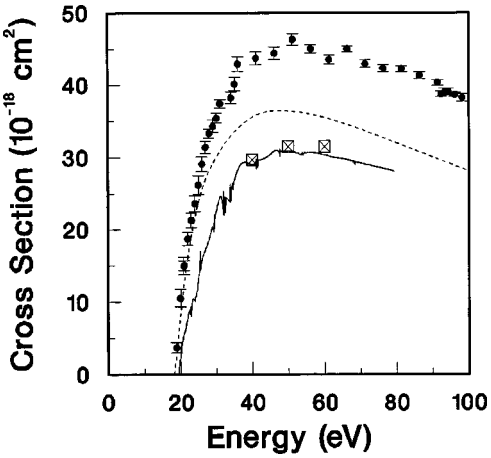


FIG. 3. Total electron-impact ionization cross section for $Be^+$. Large crossed box, time-dependent close-coupling method plus distorted-wave top up; solid curve, time-independent close-coupling method plus distorted-wave top up; dashed curve, distorted-wave method; solid circles, experimental measurements [10].

Our ionization cross section is obtained simply by summing excitation cross sections to pseudostates that lie above the ionization limit. This is formally correct when the size of the pseudostate basis tends to infinity. On using a finite basis, in principle, one should project from the pseudobound and continuum states onto the physical continuum; see, for example, [25]. If our representation of the continuum is sufficiently dense, then there is a negligible net effect on ionization due to the contribution to ionization from bound pseudostate excitation and the loss from the continuum pseudostates due to excitation of physical bound states; the two tend to cancel. This was investigated by adding an extra pseudostate per angular momentum, which resulted in an additional pseudostate per angular momentum lying in the continuum. The effect was small ($\sim +5\%$), particularly when narrow features were convoluted with a 2-eV full width at half maximum Gaussian function. This was to be expected from the convergence studies of Bray [9], the small size of the oscillations in our original results (see Fig. 3), and the agreement of our partial cross sections with the time-dependent results (see Table I).

## IV. RESULTS

Partial-ionization cross sections for $Be^+$ are presented in Table I, where we compare the close-coupling results with themselves and with distorted-wave results. The distorted-

TABLE I. Partial ionization cross sections ($10^{-18}$ cm$^2$) at an incident energy of 50 eV for $Be^+$.

| $L$ | Distorted wave results | Time-dependent close-coupling results | Time-independent close-coupling results |
|---|---|---|---|
| 0 | 0.79 | 0.72 | 0.65 |
| 1 | 3.93 | 2.11 | 2.55 |
| 2 | 5.01 | 3.78 | 3.76 |
| 3 | 3.85 | 3.03 | 2.92 |
| 4 | 5.26 | 4.41 | 4.09 |
| 5 | 5.12 | 4.98 | 4.75 |

wave method is based on a triple partial-wave expansion of the first-order perturbation theory scattering amplitude, including both direct and exchange terms. The incident and scattered electrons are calculated in a $V^N$ potential, while the bound and ejected electrons are calculated in a $V^{N-1}$ potential [26]. In previous work on the electron ionization of hydrogen [5], this choice of potentials for the distorted-wave method was found to give fairly good cross sections at high angular momentum. By $L=5$ all three methods are in reasonable agreement.

Starting with pure distorted-wave results for the total ionization cross section at 50 eV, we successively substitute the more exact close-coupling results for the low partial-wave cross sections and present them in Table II. By $L=4$ the time-dependent and time-independent methods have converged to a cross section value between 31 and 32 Mb. Even by $L=8$ the time-independent close-coupling results are still in that same range. The hybrid calculations consisting of time-dependent close-coupling results for $L=0-5$ and time-independent distorted-wave results for $L=6-30$ are compared with the converged close-coupling calculations of Bray [9] in Table III. The converged close-coupling calculations are found to be 5% higher. The principal uncertainties in the hybrid calculations are due to the choice of the core pseudopotential and the accuracy of the first-order distorted-wave calculations at the high angular momentum.

The time-dependent and time-independent close-coupling calculations for the electron-impact ionization of $Be^+$ are compared with pure distorted-wave theory and experiment [10] in Fig. 3. Both close-coupling calculations are hybrid in nature, the time-dependent close-coupling calculations make use of distorted-wave cross sections for $L=6-30$, while the time-independent close-coupling calculations are ''topped up'' by distorted-wave cross sections for $L=9-30$. The slow oscillations in the time-independent close-coupling results are due to pseudoresonances. As the basis set is increased these tend to damp to the smooth curve characteristic of direct ionization. All close-coupling calculations to date are found to lie slightly below the pure distorted-wave calculations and substantially below the experimental crossed-beam measurements [10]. We note that the first excitation-autoionization feature ($1s^2 2s \rightarrow 1s2s2p$) appears at 118 eV, well above the energy range presented in Fig. 3.

TABLE II. Total ionization cross sections ($10^{-18}$ cm$^2$) at an incident energy of 50 eV for $Be^+$. DW denotes distorted wave and CC close coupling.

| Hybrid selection | Time-dependent close-coupling results | Time-independent close-coupling results |
|---|---|---|
| DW(0→30) | 36.39 | 36.39 |
| CC(0)+DW(1→30) | 36.32 | 36.25 |
| CC(0→1)+DW(2→30) | 34.50 | 34.87 |
| CC(0→2)+DW(3→30) | 33.28 | 33.62 |
| CC(0→3)+DW(4→30) | 32.46 | 32.69 |
| CC(0→4)+DW(5→30) | 31.61 | 31.52 |
| CC(0→8)+DW(9→30) | | 31.14 |

TABLE III. Total ionization cross sections ($10^{-18}$ cm$^2$) for $Be^+$.

| Energy (eV) | Time-dependent close-coupling results | Converged close-coupling results[a] |
|---|---|---|
| 40.0 | 29.6 | 32.5 |
| 50.0 | 31.5 | 33.5 |
| 60.0 | 31.5 | 33.0 |

[a]From Ref. [9].

## V. SUMMARY

In this paper we have used the time-dependent and time-independent close-coupling methods to calculate the electron-impact ionization cross section for $Be^+$. The construction of a core pseudopotential for the time-dependent wave-packet calculations kept the lattice size relatively small and eliminated unphysical superelastic scattering. The diagonalization of the matrix of overlaps for the time-independent $R$-matrix calculations served as an efficient orthogonalization procedure for the pseudostate and continuum basis orbitals. The computer resources needed by both close-coupling methods were found to be roughly similar.

The fact that the time-dependent wave-packet method yields a magnitude for the peak ionization cross section for $Be^+$ in reasonable agreement with the three time-independent close-coupling calculations is compelling evidence that the experimental measurements need to be reexamined. The wave-packet method is essentially a numerical experiment in which asymptotic boundary conditions are not needed, unlike the time-independent formulations of scattering theory. As Bray [9] has shown, many of the low-charged ions in the Li isoelectronic sequence may also need to be revisited experimentally. Currently we are examining low-charge ions in the Na isoelectronic sequence. We stress again that the absolute magnitudes of the ionization cross sections are the crucial quantities in determining the ionization rate coefficients used in modeling many laboratory and astrophysical plasmas.

## ACKNOWLEDGMENTS

In this work, M.S.P. was supported in part by DOE Grant No. DE-FG05-96-ER54348 with Auburn University, F.R.

was supported in part by NSF Young Investigator Grant No. NSF-PHY-9457903 with Auburn University, and N.R.B. was supported in part by United Kingdom EPSRC Grant No. GR/K/14346 with the University of Strathclyde. Part of the computational work was carried out at the National Energy Research Supercomputer Center in Livermore, California and the Center for Computational Sciences in Oak Ridge, Tennessee.

[1] I. Bray and A. T. Stelbovics, Phys. Rev. Lett. **70**, 746 (1993).
[2] D. Kato and S. Watanabe, Phys. Rev. Lett. **74**, 2443 (1995).
[3] K. Bartschat and I. Bray, J. Phys. B **29**, L577 (1996).
[4] M. S. Pindzola and D. R. Schultz, Phys. Rev. A **53**, 1525 (1996).
[5] M. S. Pindzola and F. Robicheaux, Phys. Rev. A **54**, 2142 (1996).
[6] M. B. Shah, D. S. Elliot, and H. B. Gilbody, J. Phys. B **20**, 3501 (1987).
[7] I. Bray and D. V. Fursa, Phys. Rev. Lett. **76**, 2674 (1996).
[8] E. T. Hudson, K. Bartschat, M. P. Scott, P. G. Burke, and V. M. Burke, J. Phys. B **29**, 5513 (1996).
[9] I. Bray, J. Phys. B **28**, L247 (1995).
[10] R. A. Falk and G. H. Dunn, Phys. Rev. A **27**, 754 (1983).
[11] D. H. Crandall, R. A. Phaneuf, D. C. Gregory, A. M. Howald, D. W. Mueller, G. H. Dunn, D. C. Griffin, and R. J. W. Henry, Phys. Rev. A **34**, 1757 (1986).
[12] D. H. Crandall, R. A. Phaneuf and P. O. Taylor, Phys. Rev. A **18**, 1911 (1978).
[13] K. Bartschat and I. Bray, J. Phys. B **30**, L109 (1997).
[14] C. F. Fischer, Comput. Phys. Commun. **64**, 369 (1991).
[15] P. A. Christiansen, Y. S. Lee, and K. S. Pitzer, J. Chem. Phys. **71**, 4445 (1979).
[16] H. A. Yamani and W. P. Reinhardt, Phys. Rev. A **11**, 1144 (1975).
[17] I. Bray and D. V. Fursa, Phys. Rev. A **54**, 2991 (1996).
[18] N. R. Badnell, J. Phys. B **19**, 3827 (1986).
[19] P. G. Burke and K. A. Berrington, *Atomic and Molecular Processes—An R-Matrix Approach* (IOP, Bristol, 1993).
[20] K. A. Berrington, W. B. Eissner, and P. H. Norrington, Comput. Phys. Commun. **92**, 290 (1995).
[21] D. G. Hummer, K. A. Berrington, W. Eissner, A. K. Pradhan, H. E. Saraph, and J. A. Tully, Astron. Astrophys. **279**, 298 (1993).
[22] K. Bartschat, E. T. Hudson, M. P. Scott, P. G. Burke, and V. M. Burke, J. Phys. B **29**, 115 (1996).
[23] N. R. Badnell and T. W. Gorczyca, J. Phys. B **30**, 2011 (1997).
[24] T. W. Gorczyca and N. R. Badnell (unpublished).
[25] K. W. Meyer, C. H. Greene, and I. Bray, Phys. Rev. A **52**, 1334 (1995).
[26] S. M. Younger, Phys. Rev. A **22**, 111 (1980).